A regional climate model study of how biomass burning aerosol impacts land-atmosphere interactions over the Amazon

Yan Zhang,[1] Rong Fu,[1] Hongbin Yu,[2,3] Robert E. Dickinson,[1] Robinson Negron Juarez,[4] Mian Chin,[3] and Hui Wang[5]

Received 1 October 2007; revised 26 February 2008; accepted 14 March 2008; published 12 June 2008.

[1] Ensemble simulations of a regional climate model assuming smoke aerosol in the Amazon suggest that dynamic changes of cloud cover contributes to the radiative effect of the smoke on the diurnal cycles of surface fluxes and the depth and structure of planetary boundary layer (PBL). In addition to their local effects, the aerosol radiative forcing also appears to weaken or delay the circulation transition from dry to wet season, leading to a weaker moisture transport into the smoke area where the aerosols optical depth, AOD, exceeds 0.3 and a stronger moisture transport and increase of cloudiness in the region upwind to the smoke area. The land surface scheme is modified to improve the regional climate model simulation of the daily mean and diurnal cycle of the surface sensible and latent heat fluxes over the Amazon rain forest. The aerosol radiative forcing is applied to the model during a dry to wet transition season (August–October) in that region. Cloudiness decreases in early afternoon due to the absorption of solar radiation by smoke aerosols partially compensate for the reduction of surface solar flux by aerosol scattering, shifting the strongest changes of surface flux and the PBL to late morning. The reduction of net solar radiation at the surface by smoke is locally largely compensated by reduction of surface sensible flux, with reduction of latent flux only about 30% as large. The strong aerosol absorption in the top 1 km of the aerosol layer stabilizes the 2 to 3 km layer immediately above the daytime PBL and consequently cloudiness decreases. This reduced surface solar flux and more stable lapse rate at the top of the PBL stabilize the lower troposphere. These changes lead to anomalous wind divergence in the southern Amazon and anomalous wind convergence over the equatorial western Amazon in the upwind direction of the smoke area.

Citation: Zhang, Y., R. Fu, H. Yu, R. E. Dickinson, R. N. Juarez, M. Chin, and H. Wang (2008), A regional climate model study of how biomass burning aerosol impacts land-atmosphere interactions over the Amazon, *J. Geophys. Res.*, *113*, D14S15, doi:10.1029/2007JD009449.

1. Introduction

[2] Smoke aerosols released from biomass burning absorb and scatter solar radiation, consequently changing the surface energy and water fluxes, the atmospheric thermodynamic stability, and thereby cloud formation. These effects are referred to the aerosol direct and semidirect effects [*Charlson et al.*, 1992; *Hansen et al.*, 1997]. Smoke aerosols also act as cloud condensation nuclei to change reflectivity and lifetime of cloud drops. That influence is referred to as the aerosol indirect effect [*Twomey*, 1977]. Many previous studies have shown that these changes can affect the occurrence and distribution of clouds and atmospheric convection [e.g., *Kaufman et al.*, 1998; *Andreae et al.*, 2004], but relatively few studies have examined whether or not and how smoke aerosols might affect the regional circulation, especially the circulation transition from the dry to wet season.

[3] The concentration of smoke aerosol over the Amazon forest peaks during the transition from dry to wet season. The influence of aerosols on clouds and convection in this region has been investigated extensively through recent field experiments, e.g., the Large-Scale Biosphere-Atmosphere Experiment in Amazonia-Smoke, Aerosols, Clouds, Rainfall, and Climate (LBA-SMOCC), Smoke/Sulfates, Clouds and Radiation-Brazil (SCAR-B), ground based operational aerosol observational network (AERONET), and satellite observations [*Andreae et al.*, 2004; *Koren et al.*, 2004; *Kaufman et al.*, 1992, 1998; *Kaufman and Koren*, 2006]. Other studies have modeled aerosol induced cloud changes [*Feingold et al.*, 2005; *Liu*, 2005]. Most of these

[1]School of Earth and Atmospheric Sciences, Georgia Institute of Technology, Atlanta, Georgia, USA.
[2]Goddard Earth Science and Technology Center, University of Maryland, Baltimore County, Baltimore, Maryland, USA.
[3]Laboratory for Atmospheres, NASA Goddard Space Flight Center, Greenbelt, Maryland, USA.
[4]Department of Ecology and Evolutionary Biology, Tulane University, New Orleans, Louisiana, USA.
[5]Wyle Information Systems, Climate Prediction Center, NOAA, Camp Springs, Maryland, USA.

Copyright 2008 by the American Geophysical Union.
0148-0227/08/2007JD009449

studies have focused on how aerosols influence cloud microphysics [*Andreae et al.*, 2004; *Feingold et al.*, 2005] or local thermodynamics at scales of a cloud or a convective complex [*Yu et al.*, 2002; *Liu*, 2005].

[4] Various studies have suggested a variety of semidirect and indirect influences of smoke aerosols on the large-scale cloud distribution [*Ackerman et al.*, 2000; *Andreae et al.*, 2004; *Koren et al.*, 2004; *Kaufman and Koren*, 2006; *Yu et al.*, 2007]. The semidirect effect of smoke aerosols may either increase or decrease clouds locally and remotely. Numerical simulations addressing the aerosol semidirect effect have included the use of large eddy simulations, regional climate models, and global climate models [*Feingold et al.*, 2005; *Johnson et al.*, 2004; *Liu*, 2005; *Huang et al.*, 2006; *Menon et al.*, 2002]. While the large-eddy simulations can provide in-depth and detailed pictures as to how smoke aerosols can affect surface fluxes and cloud lifetime, they are limited to short simulation periods and small geographic domains because of their high computational cost. A global climate model, on the other hand, cannot adequately resolve sharp changes of topography in regions such as the Andes. Thus a regional climate model balances the need for resolving the sharp topographic gradients of the Andes with the use of a domain large enough to include the possible response of transport of water vapor over the ocean to aerosol forcing, and applied over several months of the transition period from dry to wet season.

[5] The diurnal cycle of surface fluxes is important for the formation of clouds and convection over land. Smoke aerosols through their modification of solar radiation, impact the diurnal changes of surface fluxes and the evolution of the planetary boundary layer (PBL). Understanding these impacts is important for determining the radiative influence of aerosols on clouds and convection over South America. *Yu et al.* [2002] have examined such impacts by using a single column PBL model with idealized aerosol radiative forcing. However, such a model cannot address how the aerosol would influence regional circulation through changes in horizontal temperature, pressure gradient, and advection nor how such changes in turn would affect clouds away from the smoke area. This study examines these questions as a first step toward understanding the semidirect effect of aerosols on surface energy and water fluxes, PBL structure, and clouds during the transition from dry season to monsoon onset.

[6] *Liu* [2005] used a regional climate model to simulate atmospheric response and feedback to radiative forcing from smoke aerosols during dry to wet transition season. That study modeled a land surface that was too dry during the transition season compared to observations. It used a spatially uniform aerosol optical depth (AOD, 0.75) and single scattering albedo (SSA, 0.88, 0.82, and 0.94, respectively) based on the SCAR-B field campaign as the smoke aerosol forcing. Daily mean results from a single simulation for the control and aerosol experiment, respectively, were analyzed to examine the aerosol influence. The present study examines with ensemble simulations the influence of smoke aerosols on the diurnal changes of the surface fluxes, clouds, and the PBL height. It uses improved surface climate conditions in the regional model, and its aerosol radiative forcing includes spatially varying AOD and SSA.

[7] The model and design of simulations are described in section 2. Section 3 describes modification of land surface processes and evaluation of the surface fluxes for the regional climate model. The results of model simulations are presented in section 4, and the discussion and conclusions are given in sections 5 and 6, respectively.

2. Model and Methods

2.1. Model Description

[8] This study applies the Abdus Salam Institute for Theoretical Physics Regional Climate Model, version 3 (RegCM3) [*Pal et al.*, 2007; *Qian and Giorgi*, 1999]. This model can well simulate the interannual variability in the timing of the rainy season [*Rauscher et al.*, 2007]. It is driven by the National Center for Environmental Prediction (NCEP) Reanalysis data sets for initial and boundary conditions. More realistic large-scale boundary conditions over South America for the RegCM3 might be obtained from ECMWF reanalysis. But this reanalysis ends in August 2002 and thus does not fully overlap with our study time period. The objective of this study is to diagnose the mechanisms through which the aerosol direct and semidirect effects influence the surface atmosphere and regional circulation instead of attempting a realistic simulation. Thus the selection of initial and boundary conditions should not qualitatively affect our conclusions.

[9] The radiative transfer scheme is similar to that in the National Center for Atmospheric Research Community Climate Model (CCM3) [*Kiehl et al.*, 1998]. For solar radiative transfer calculations, RegCM3 uses the δ-Eddington approximation [*Briegleb*, 1992] to account for large forward scattering by clouds and aerosols. This scheme determines the cloud influence on solar radiation by three cloud parameters: fractional cover, water content and effective radius of cloud droplets. The aerosol direct effect is calculated with three quantities: extinction optical depth, single scattering albedo, and asymmetry parameter; all are functions of wavelength. Interactions of aerosol with thermal infrared radiation are not included in the model, because smoke aerosol optical depth decreases rapidly with increasing wavelength. The dynamic core of RegCM3 is similar to that of the hydrostatic version of the fifth-generation Pennsylvania State University-National Center for Atmospheric Research (PSU-NCAR) Mesoscale Model (MM5) [*Grell et al.*, 1994]. Its moist convection and precipitation are parameterized by the *Grell* [1993] cumulus scheme. Sea surface temperatures (SST) are prescribed over the ocean with monthly averages of measurements. The scheme for land is based on an earlier version of the Biosphere-Atmosphere Transfer Scheme [*Dickinson et al.*, 1993] and is employed to compute surface net solar radiation, sensible and latent heat fluxes, momentum fluxes, and surface temperature from prescribed vegetation and soil types.

2.2. Simulation Design

[10] The choice of model domain in a regional climate model simulation can influence model sensitivity to various internal and external forcings [*Seth and Giorgi*, 1998]. This study includes tropical and subtropical South America and the surrounding oceans (80°W $\sim$ 20°W, 35°S $\sim$ 5°N) as

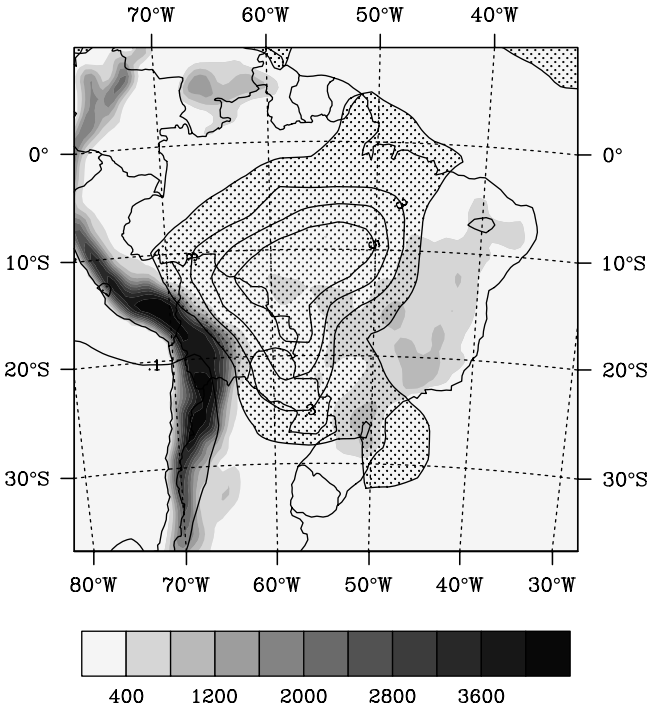

Figure 1. The domain of the RegCM3 simulation. Topography (m) is indicated by gray shades. Distribution of AOD at 550 nm for September 2002 is derived from an integration of MODIS retrievals and GOCART simulations as described by *Yu et al.* [2003]. The AOD interval of 0.1 from 0 to 0.6 is indicated by contour, and the area with AOD > 0.2 are shaded by dots.

illustrated in Figure 1 for the simulation domain. The area of this domain is about 5400 × 5400 km^2, which is large enough to avoid the influence of domain boundary on simulated atmospheric fields inside of the Amazon basin. Its atmosphere has 18 levels, with 7 levels in the lowest 1.5 km of atmosphere, and a horizontal resolution of 60 km.

[11] For this study, we choose the period of August to October 2002 as the peak season for burning in South America. Satellite observation of clouds and aerosols from the Moderate Resolution Imaging Spectroradiometer (MODIS) on the EOS-Aqua satellite showed a clear signal of reduced warm cloud fraction with increasing AOD over the Amazon in 2002, implying a dominance of "cloud burning" as expected from the aerosol semidirect effect [*Koren et al.*, 2004; *Yu et al.*, 2007]. This study used monthly averaged aerosol fields from a combination of the MODIS retrievals and the Goddard Chemistry Aerosol Radiation and Transport (GOCART) model simulations to achieve an optimal geographical distribution of AOD [*Yu et al.*, 2003]. Figure 1 shows distributions of AOD at 550 nm for September. The spatial distributions of the SSA and asymmetry parameter (g) are obtained from GOCART simulations [*Chin et al.*, 2002]. Averaged over the smoke region, the aerosol SSA is about 0.86 and g is about 0.7. These values do not have large spatial variation in the region of our study. This value of SSA is much smaller than that obtained from AERONET retrievals [*Dubovik et al.*, 2002] but is within the large range of in situ measurements for aged regional smoke as summarized by *Reid et al.* [2005]. The GOCART simulations are only available for 2001, and their aerosol forcing could be somewhat weaker than the smoke aerosol forcing during August–October of 2002 [*Procopio et al.*, 2004; *Yu et al.*, 2007]. However, the use of the GOCART aerosol radiative forcing for our simulations should not change the processes through which aerosol radiative effect influences regional surface energy and water fluxes and circulation.

[12] The aerosol effects over the Amazon region are examined with two sets of ten-member ensemble experiments. Ten ensemble simulations reduce the random error of the surface solar flux over the smoke area where AOD $\geq$ 0.3 to 4 W m^{-2}, significantly less than the difference between the aerosol and control simulations (24 W m^{-2}). For each modeling experiment, RegCM3 is integrated from August to October when biomass burning is most active and the transition to monsoon takes place. August as a spin-up period is excluded from the analysis. Discussion of aerosol effects is focused on September when smoke aerosol has maximum loading.

[13] The first set of the ensemble experiments is a control run without including aerosol, and is referred to as CONT hereinafter. These ensemble experiments were initiated with different dates varying from 1 to 10 August 2002, respectively. The second set of the ensemble experiments uses the same initial and boundary conditions as for the CONT experiment, but is forced by aerosol radiative effects, which in turn influence atmospheric and surface heating and clouds in RegCM3. This set of experiments is referred to as AERO hereinafter. A well mixed aerosol layer is placed from the surface to 3 km height in these simulations, as suggested by aircraft and satellite observations of the vertical range of smoke layer over the Amazon [*Andreae et al.*, 2004; *Landulfo et al.*, 2003; *Chand et al.*, 2006; *Yu et al.*, 2007; *Labonne et al.*, 2007].

[14] The impact of aerosols radiative forcing is estimated as the difference between two ensemble experiments ($\Delta \equiv$ AERO-CONT). Aerosol radiative forcing changes the lapse rate, water vapor, and cloud in our simulations. These changes together with the direct radiative effects of aerosol affect the surface fluxes and PBL structure.

3. Modification and Evaluation of the Model

3.1. Modification of Land Surface Properties

[15] Observations show that roots of the tropical forest in the Amazon could reach as deep as 14 to 18 m and are capable of transpiring considerable amounts of water throughout the dry season [*Nepstad et al.*, 1994]. In the RegCM3 model, the default depth of soil and root layer for tropical forest is set to 3 m and 1.5 m, respectively. Such a shallow soil layer could not retain enough moisture to support realistic evapotranspiration (ET) in the Amazon. As a result of this problem, the model is known to substantially underestimate surface latent heat flux during the transition season [*Gash and Nobre*, 1997]. Similar to that done by *Kleidon and Heimann* [2000], we used deeper rooting depths for a tropical forest to mitigate this problem. The depth of soil and root layer for a tropical forest was increased to 4.5 m and 3 m, respectively. We also changed the ratio of root distribution between the upper soil layer

Table 1. Comparison of Monthly Mean Sensible Heat (SH), Latent Heat (LH), Bowen Ratio (BR = SH/LH), Surface Net Solar Radiation (SR), and 2 m Air Temperature (T) Between RegCM3 Simulations and Measurements by Flux Tower for September 2002[a]

Sites	Variables	RegCM3 Simulations: Original Land Scheme	RegCM3 Simulations: Modified Roots Land Scheme	RegCM3 Simulations: Modified Roots Land Scheme With Aerosols	Flux Tower Observations
Tapajos (3.01°S, 54.58°W)	SH	110	42	40	33
Tapajos (3.01°S, 54.58°W)	LH	29	120	113	101
Tapajos (3.01°S, 54.48°W)	BR	3.8	0.35	0.35	0.33
Tapajos (3.01°S, 54.48°W)	SR	216	212	180	225
Tapajos (3.01°S, 54.48°W)	T	304.7	300.6	299.8	300.3
Ji Parana (10.07°S, 62.93°W)	SH	83	42	27	28
Ji Parana (10.07°S, 62.93°W)	LH	54	104	101	99
Ji Parana (10.07°S, 62.93°W)	BR	1.5	0.40	0.27	0.28
Ji Parana (10.07°S, 62.93°W)	SR	198	202	200	220
Ji Parana (10.07°S, 62.93°W)	T	306.8	300.7	300.0	299.0

[a]Units for sensible heat, latent heat, and surface net solar radiation are W m^{-2}, and units for air temperature are K.

(0.1 m) and root zone soil layer (3 m) from 0.8 to 0.4, such that more roots are allocated in the root zone soil layer. These modifications have increased the availability of water for root uptake and improved the daily mean surface fluxes. Table 1 compares the monthly mean sensible heat flux (SH), latent heat flux (LH), surface net solar radiation (SR), Bowen ratio (BR = SH/LH), and surface temperature (T) obtained from three sets of RegCM3 simulations and those from flux tower observations during September 2002 at two tropical forest sites in Brazil, namely Tapajos (3.01°S, 54.58°W, denoted as K83) and Ji Parana (10.07°S, 62.93°W, denoted as RJA) [*von Randow et al.*, 2004; *da*

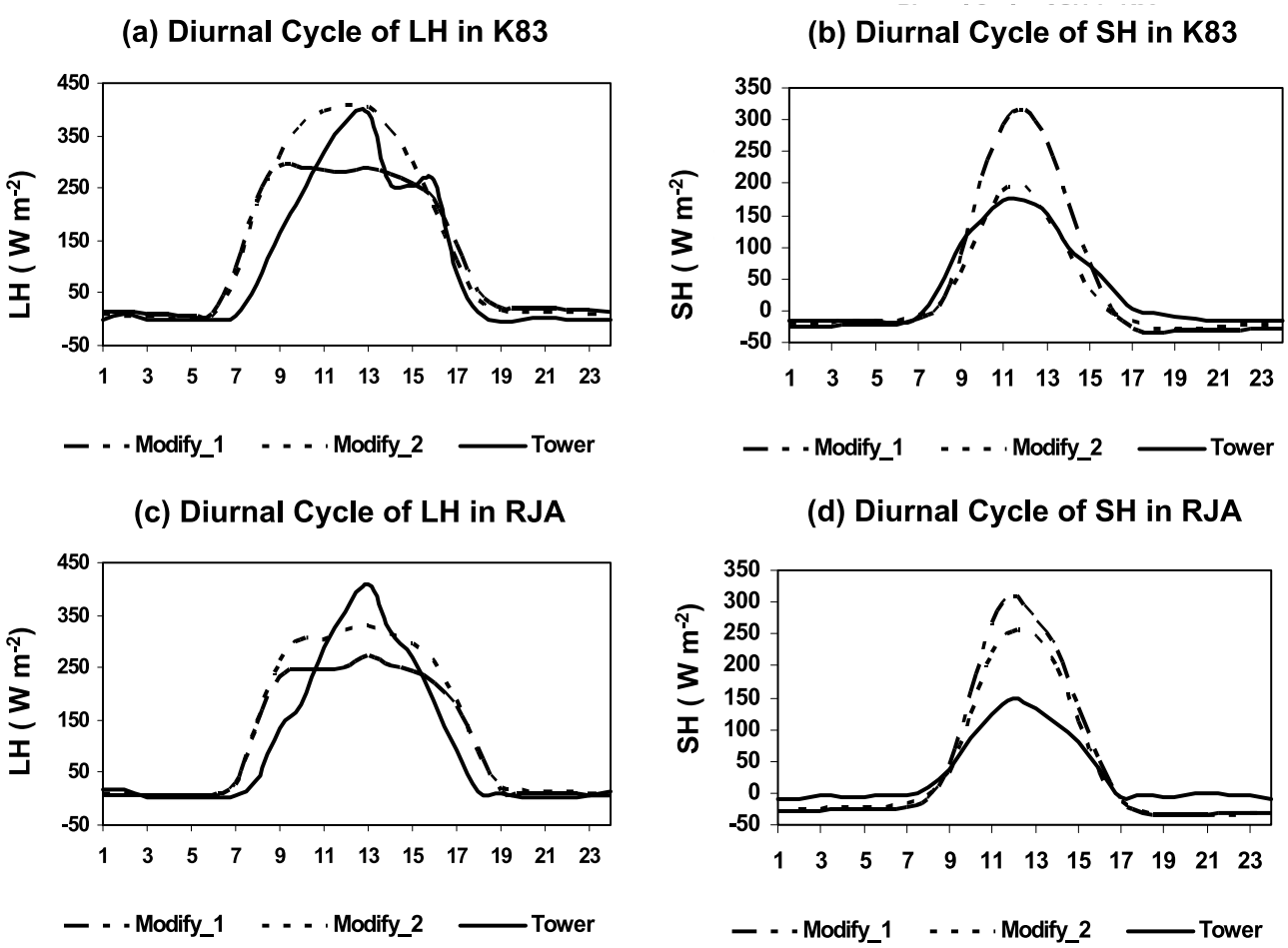

Figure 2. Comparison of the diurnal cycle of LH and SH (W m^{-2}) between RegCM3 simulations and in situ observations. Modify_1 represents a simulation using root modified RegCM3, and Modify_2 represents a simulation with modified root and soil moisture treatment as described in section 3.1; Tower represents observations by flux tower. K83 denotes Tapajos, and RJA denotes Ji Parana. (a) LH K83, (b) SH K83, (c) LH RJA, and (d) SH RJA.

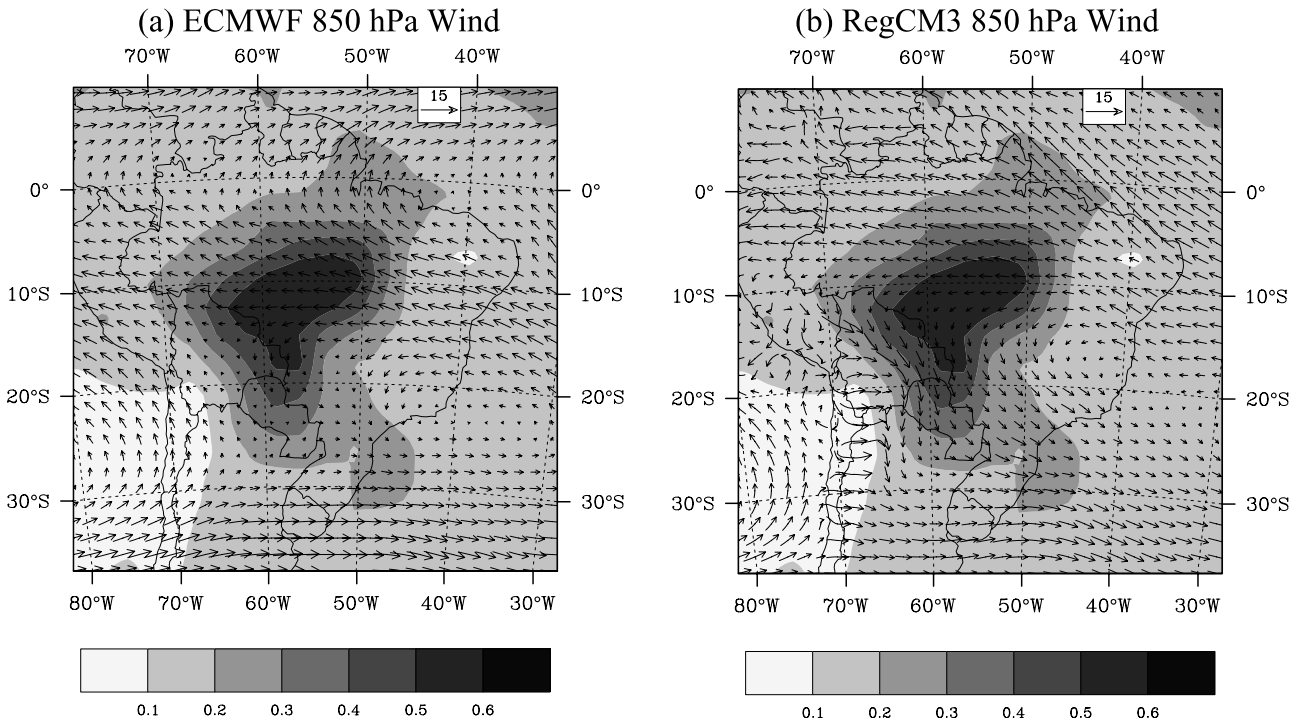

Figure 3. Monthly mean 850 hPa wind vector (m s^{-1}) obtained from ECMWF short-term forecast product and RegCM3 for September 2002 and aerosol optical depth shown by gray shaded patterns.

Rocha et al., 2004; *Goulden et al.*, 2004]. The simulated surface solar fluxes agree with observations within 10–20%. However, the original RegCM3 land scheme overestimates the sensible heat flux and underestimates the latent heat flux substantially, leading to a Bowen ratio of 3.8, an order of magnitude larger than the observed value of 0.33. The use of deeper root depths increases the ET and reduces the sensible heat flux, yielding a Bowen ratio that is in good agreement with measurements. Inclusion of the aerosol radiative forcing brings the Bowen ratio yet closer to the observations.

[16] The formation of shallow clouds and deep convection strongly depend on the depth and static stability of the daytime PBL [*Williams and Renno*, 1993; *Fu et al.*, 1999; *Betts and Jakob*, 2002]. The latter is controlled by diurnal changes of the surface fluxes. Figure 2 shows the diurnal cycle of SH and LH for September from RegCM3 simulation and tower observations. Clearly, RegCM3 with the modified root depth and vertical distribution still overestimates SH and underestimates LH during the daytime, especially at noon when the solar radiation is at its maximum. Thus simply increasing root zone depth and its fraction in deeper soil of the model cannot alone provide sufficient soil moisture to support a realistic daily maximum LH. Observations over the Amazon forest near Manaus in September 1995 showed that the soil moisture content in the upper 4 m of soil was about 1900 mm [*Malhi et al.*, 2002], whereas averaged total forest soil water content in the 3 m layer of RegCM3 is only about 1000 mm. Given our focus on obtaining realistic surface fluxes rather than on improving the physics of the land surface process, we fixed the soil moisture in the root layer to be 80% of the field capacity over the tropical forest area. This modification fixes soil water in the forest root zone at approximately 1.4 m, consequently enabling RegCM3 to obtain a more realistic daily mean of the land surface fluxes and an improved diurnal cycle of these fluxes over the Amazon during the transition season (Figure 2).

3.2. Evaluation of the RegCM3

[17] Figure 3 shows the 850 hPa wind field from the ECMWF short-term forecast product and RegCM3 CONTS simulations. The simulated pattern of wind in the RegCM3 is similar to that of ECMWF, but its simulated wind speed is weaker over southern Amazonia. The spatial pattern of change of geopotential height at 500 hPa from September to October, a main indicator of the transition from dry season to the monsoon onset, is well simulated in the RegCM3 (Figure 4).

4. Simulated Aerosol Influences

[18] This section evaluates the smoke aerosol direct and semidirect effects by comparing the results of the ensemble AERO and CONT simulations. Unless stated otherwise, all variables in the analysis are averaged over September at the peak of biomass burning.

4.1. Radiation and Surface Fluxes

[19] The aerosol radiative forcing calculated at the top of atmosphere (ΔF_{TOA}, positive value for downward radiative flux) for clear-sky and whole-sky conditions are shown in Figures 5a and 5b, respectively. Smoke aerosols reflect solar radiation back to the space resulting in a negative ΔF_{TOA}. They also absorb solar radiation. Such aerosol absorption of solar radiation reduces the planetary albedo and contributes

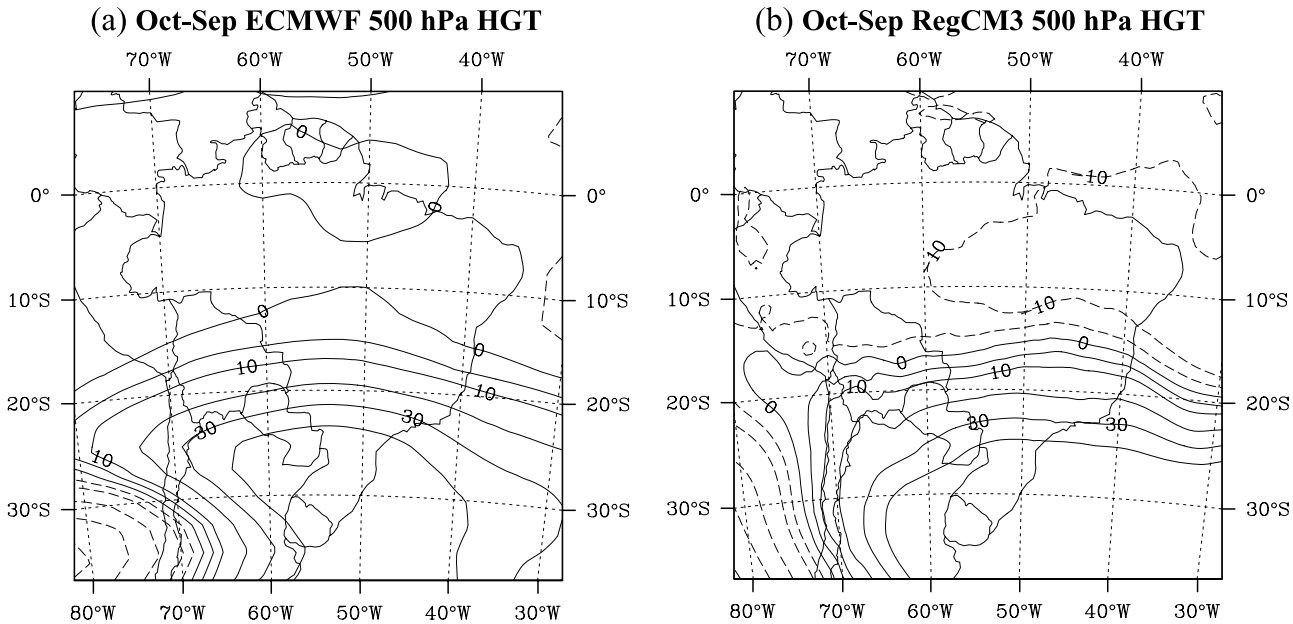

Figure 4. Monthly averaged 500 hPa geopotential height (units are m) derived from ECMWF short-term forecast product and RegCM3 for difference between October and September 2002 and aerosol optical depth shown by color shaded patterns.

to a positive ΔF_{TOA}. Thus the influences on ΔF_{TOA} from scattering and from absorption by smoke aerosols oppose each other. For a darker land surface and for clear-sky, the reflection is larger, and consequently $\Delta F_{TOA,clear}$ is negative with a spatial distribution that is similar to that of the AOD distribution and peaking at approximately -8 W m^{-2} over the maximum AOD region (Figure 5a). For a bright surface, i.e., where there is snow cover over the Andes Mountains, the planetary albedo is reduced by the smoke aerosols and the forcing is positive.

[20] The whole-sky radiative forcing ($\Delta F_{TOA,total}$) is affected by both aerosol scattering and absorption and change of cloud properties, i.e., fractional cover and cloud liquid water path. Therefore its pattern (Figure 5b) does not necessarily match that of the AOD distribution. Indeed, the peak magnitudes of $\Delta F_{TOA,total}$ ($\sim \pm$ 22 W m^{-2} relative to 8 W m^{-2} uncertainty due to random errors of the ensemble simulations) are several times as large as the clear sky negative value indicating dominance by the cloud property changes. The role of cloud contributions to $\Delta F_{TOA,total}$ is isolated in Figure 5c by subtracting it from $\Delta F_{TOA,clear}$ showing it to be positive (i.e., a decrease of cloud fraction or cloud liquid water) over most of the Amazonian region but negative (increases cloudiness) over northwestern Amazonia.

[21] Figure 6 shows change of the solar radiative forcing by aerosols at the surface ($\Delta F_{Surface}$) for clear-sky and whole-sky, positive for a reduction of cloud fraction or liquid water path. Both the scattering and absorption of the smoke aerosols decrease the amount of solar energy at the surface by as much as 40 W m^{-2} (or 15%) for clear-sky conditions over the central Amazon. The spatial pattern of $\Delta F_{Surface,clear}$ generally follows that of AOD. For whole-sky conditions, the spatial pattern differs as reduction of SR ($\Delta F_{Surface,total}$) by smoke aerosols and is compensated by the reduction in cloud fraction that allows more solar radiation to reach the surface and thereby weakens aerosol direct radiative effect, mostly over the smoke areas (30 W m^{-2}) where AOD > 0.3. The whole-sky surface solar radiation reduction over the smoke area is about 10 W m^{-2} less than the clear-sky reduction.

[22] The forcing efficiency, defined by the aerosol forcing in clear-sky normalized by the AOD, is about $-10 \sim -15$ W m^{-2}/AOD for clear-sky at the TOA and $-70 \sim -80$ W m^{-2}/AOD at the surface (figure not shown). The TOA values are in the lower end of the published range but the surface values are consistent with AERONET and other measurements [*Yu et al.*, 2006; *Zhou et al.*, 2005; *Procopio et al.*, 2004].

[23] The change of solar heating changes atmospheric stability and surface heat fluxes. Figure 7 shows the consequent perturbations of surface fluxes of sensible heat (SH) and latent heat (LH). A reduction of SH of up to 25 W m^{-2} occurs primarily over the smoke area (AOD > 0.3). That largely balances the reduction of net solar flux. The reduction of LH is weaker, in part because of an increase of vegetation transpiration near local noon, and has no obvious pattern.

4.2. Planetary Boundary Layer Evolution

[24] The influence of smoke aerosols on the diurnal cycle of the surface fluxes and on the PBL are examined by area mean changes of these variables over the smoke center, i.e., where AOD > 0.3.

[25] Figure 8 shows the diurnal variation of the clear-sky and whole-sky surface solar fluxes (SR), respectively, in the CONT experiment as well as the changes due to the radiative effect of smoke aerosols. Without smoke aerosols, SR reaches a maximum at noon for both cases. The total cloud forcing, i.e., the difference between whole-sky and

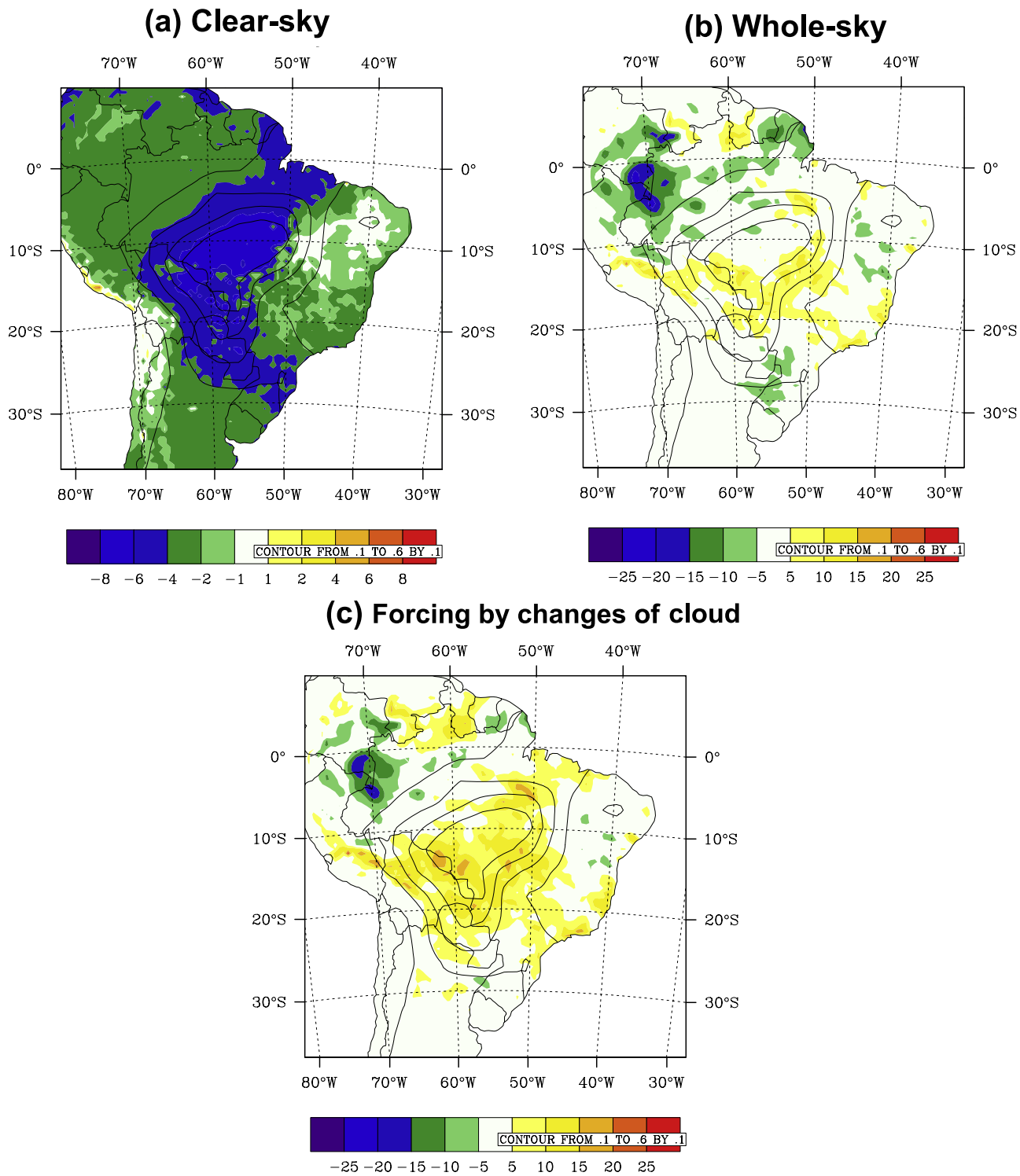

Figure 5. Difference in monthly daily mean TOA net downward solar radiation (W m^{-2}) between AERO and CONT for (a) clear-sky condition, (b) whole-sky condition, and (c) the TOA forcing by changes in cloud properties.

clear-sky SR, is as much as −200 W m^{-2} in the afternoon. With aerosols, SR at the surface for clear-sky is reduced by about 80 W m^{-2} from 0800 LST to 1500 LST. For whole-sky, this aerosol forcing is weakened because of cloud reduction between 1300 LST and 1700 LST.

[26] Figure 9 shows the aerosol induced changes of SR and net outgoing infrared radiation (LW), as well as those of SH and LH. In general, reduction of SR is mostly balanced by reduction of SH, and only secondarily, by changes of LH and LW. SH decreases significantly during the day with its

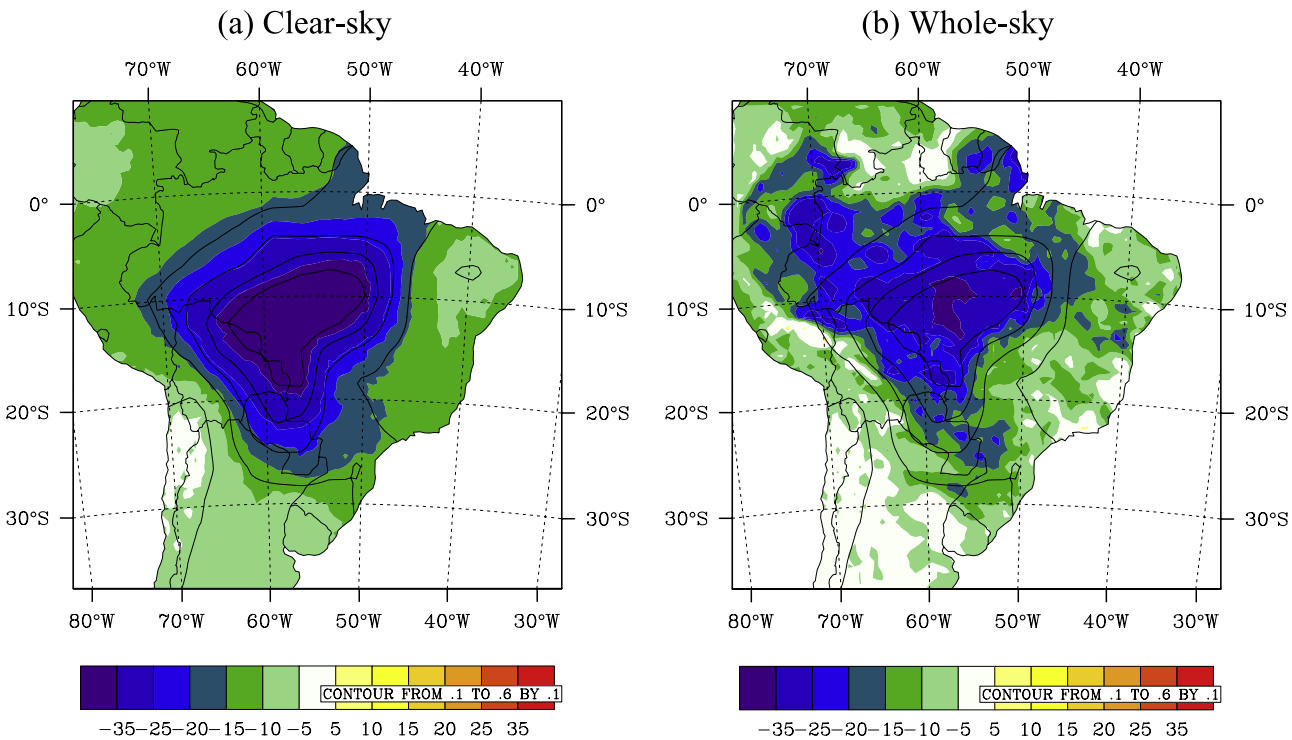

Figure 6. Difference of monthly average solar flux (W m^{-2}) at surface between AERO and CONT for (a) clear-sky condition and (b) whole-sky condition.

largest reduction of about 70 W m^{-2} (25%) at 1100 LST. Daily average changes of SH and LH in the selected domain are −15 W m^{-2} and −5 W m^{-2}, respectively. The LH change is about 1/3 of the SH change, so the Bowen ratio is lowered by 0.14 (about 30%). The model determines SH over vegetation by the difference of air temperature between that within and that above the foliage. The reduction of SH is related to a greater reduction of leaf surface temperature

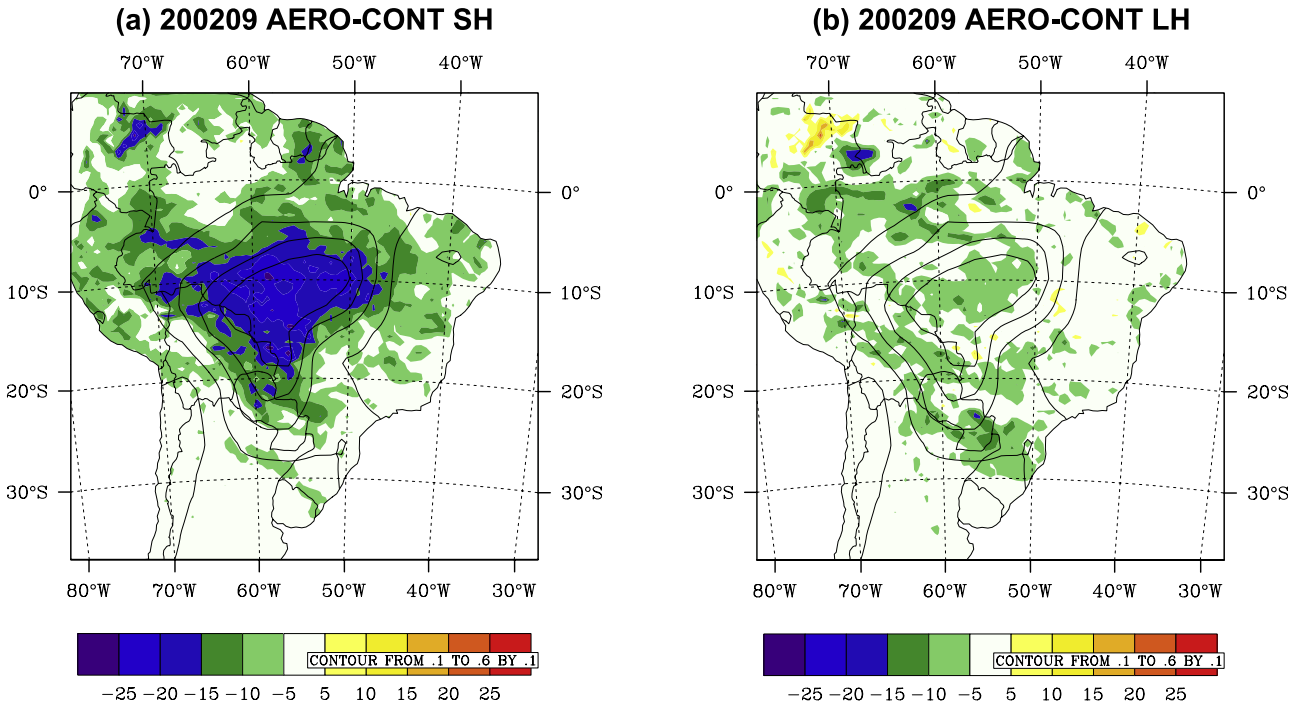

Figure 7. Difference of (a) monthly average sensible heat flux (SH, W m^{-2}) and (b) monthly average latent heat flux (LH W m^{-2}) between AERO and CONT simulations.

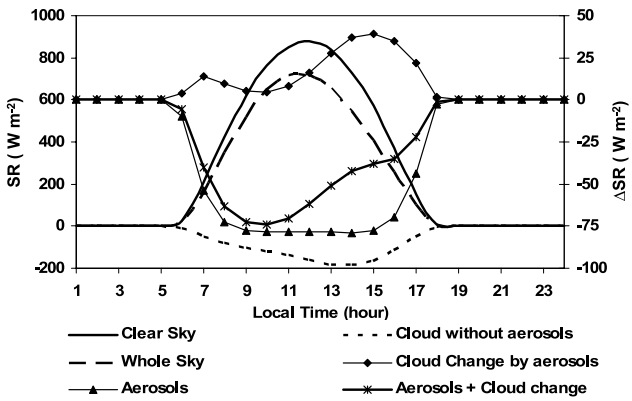

Figure 8. Diurnal cycle of surface net solar flux SR (left axis) and its change induced by smoke aerosols, aerosol induced cloud changes, and smoke aerosols plus cloud changes (right axis) averaged over area where ADO > 0.3 in September. Units are W m^{-2}.

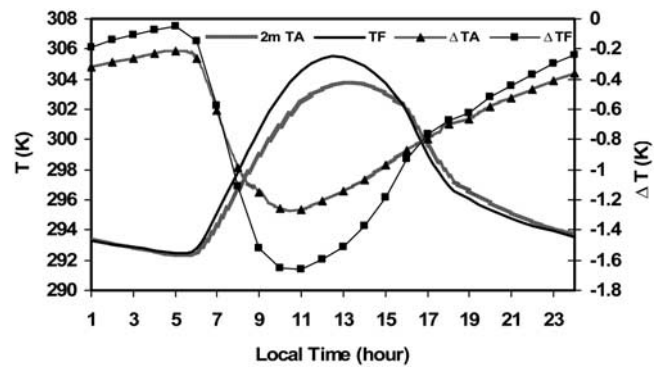

Figure 10. Diurnal cycle of foliage surface temperature (TF) and air temperature (TA) at 2 m (left axis, solid curves) and their changes due to aerosols (right axis, solid curves with symbols) averaged over area where ADO > 0.3 in September.

than the reduction of air temperature above. As shown in Figure 10, the leaf surface temperature is reduced by the aerosol cooling effect by as much as 1.7°C at 1100 LST, whereas the air temperature reduction at 2 m above the foliage is only 1.3°C.

[27] Why does LH decrease in early morning and late afternoon, but increase from late morning to early afternoon (Figure 9)? Figure 11 shows that the evaporation from canopy interception increases uniformly, presumably because of the increase in precipitation. This term is more than compensated by a decrease in transpiration in the early morning and late afternoon. But during late morning to early afternoon, transpiration increases slightly in the presence of aerosols, leading to a small increase in LH. The cooler midday temperature in the presence of aerosols reduces the midday vapor pressure term and so decreases the stomatal resistance, hence increases the transpiration [*Steiner and Chameides*, 2005].

[28] Diurnal changes in the height of the PBL are determined by the surface buoyancy flux and capping inversion. Smoke aerosols reduce the surface SH and convectively driven turbulence, and also warm the lower troposphere. These effects can strengthen the capping inversion and decrease the height of the daytime PBL [*Yu et al.*, 2002]. Previous field measurements in the Southern Amazon suggest that the daily maximum height for PBL varies from 250 m to 1.25 km over forests and from 110 m to 2.22 km over pasture during dry season [*Nobre et al.*, 1996]. Figure 12 shows that the PBL in our simulations varies from 400 m to 2 km. The simulated daily maximum PBL height is about 500 m higher than that observed over forest. This discrepancy is in part caused by an overestimate of daily maximum surface sensible flux, and presumably also by a weakness in the treatment of PBL physics. Given the model's tendency to overestimate surface sensible flux, the change of PBL due to smoke aerosols radiative forcing may also be overestimated. The smoke aerosols delay the growth of the PBL in the morning and reduce its daytime height. The maximum reduction of the PBL height is about 300 m (16%) and occurs at 1100 LST, much larger than the 40 m uncertainty due to random errors of ensemble simulations. The change of the PBL height in the late afternoon is not as

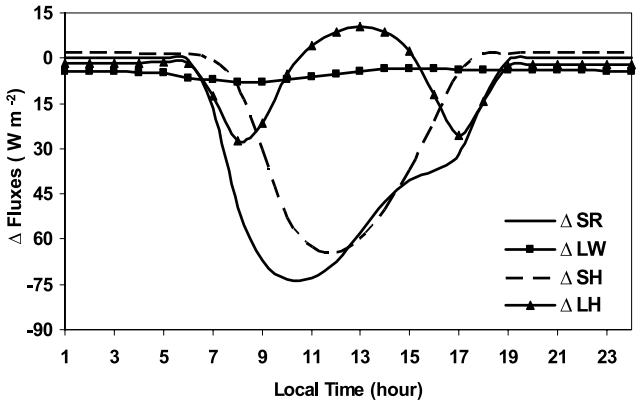

Figure 9. Diurnal cycle of changes of surface net solar radiation (ΔSR), outgoing infrared radiation (ΔLW), sensible heat flux (ΔSH), and latent heat flux (ΔLH). Units are W m^{-2}.

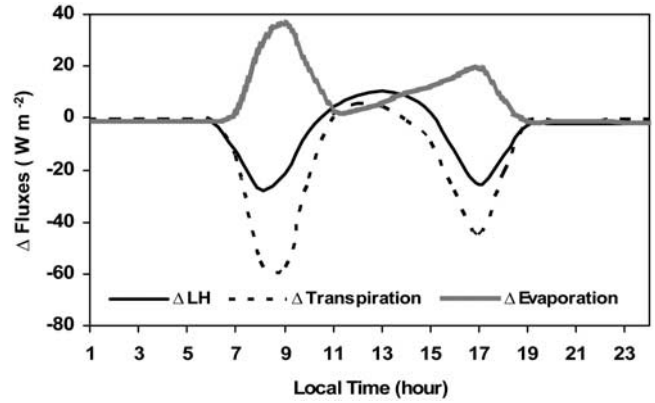

Figure 11. Diurnal cycle of the change in surface latent heat flux (ΔLH) and its transpiration (ΔTranspiration) and evaporation (ΔEvaporation) component between the AERO-CONT simulations averaged over area where ADO > 0.3 in September.

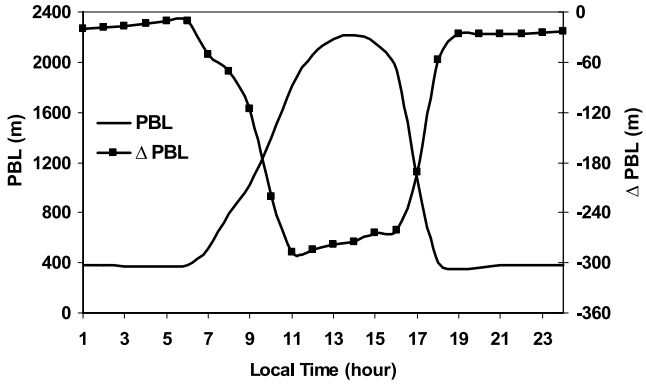

Figure 12. Diurnal evolution of the planetary boundary layer (PBL) height (left axis, solid curve) and its change due to aerosols (right axis, solid curve with symbol) averaged over area where ADO > 0.3 in September.

strong as in the morning, consistent with the weaker reduction of the SH due to "cloud burning." The weaker influence of aerosols on the PBL height in early afternoon is consistent with the weaker reductions of SR and SH (Figure 9).

4.3. Effect on Clouds

[29] Smoke aerosols can affect atmospheric thermodynamics by absorbing solar radiation and consequently can influence the cloud fraction through the following processes: (1) by decreasing surface sensible flux and increasing atmospheric stability and thus reducing turbulence, (2) by changing the relative humidity (RH) either due to changing dry air entrainment at top of the PBL or due to changing temperature, and (3) by changing horizontal pressure gradient and regional circulation.

[30] Figure 13a shows the spatial distribution of the difference (AERO-CONT) in cloud liquid water path (LWP) integrated between the surface and 2 km and the difference of the wind at 1.5 km within the daytime PBL. No obvious change in the cloud LWP within the daytime PBL appears in the smoke areas. However, in equatorial Amazonia to the north and northwest of the smoke area, cloud LWP increases by as much as 20 g m^{-2} or 40% to 50%. Figure 13b shows the changes of cloud LWP for the layer from 2 km to 3 km and the change of wind at 3 km for the AERO-CONT. A large-scale decrease of cloud LWP between 2 and 3 km layer can be seen both inside and to the north of the smoke areas. However, over equatorial Amazonia to the north of the smoke area, the increase of cloud LWP below 2 km more than compensates for the reduction of cloud LWP above 2 km, leading to a net increase of cloud LWP in that region. Within the smoke area, the vertically integrated LWP decreases as a result of direct and semidirect effect of smoke aerosols. In October (figure not shown), the pattern of cloud LWP change is similar to that in September. Cloud LWP between the surface and 2 km increases by as much as about 23 g m^{-2} to the northwest of the smoke area, and cloud LWP between 2 and 3 km decreases (by about 10 g m^{-2}) in the smoke area.

[31] What might cause the changes of LWP shown in Figure 13? Aerosols are prescribed to be vertically uniform within the smoke area. However, the solar radiation absorbed by smoke aerosols is strongest at the top of the smoke layer. This aerosol absorption increases the air

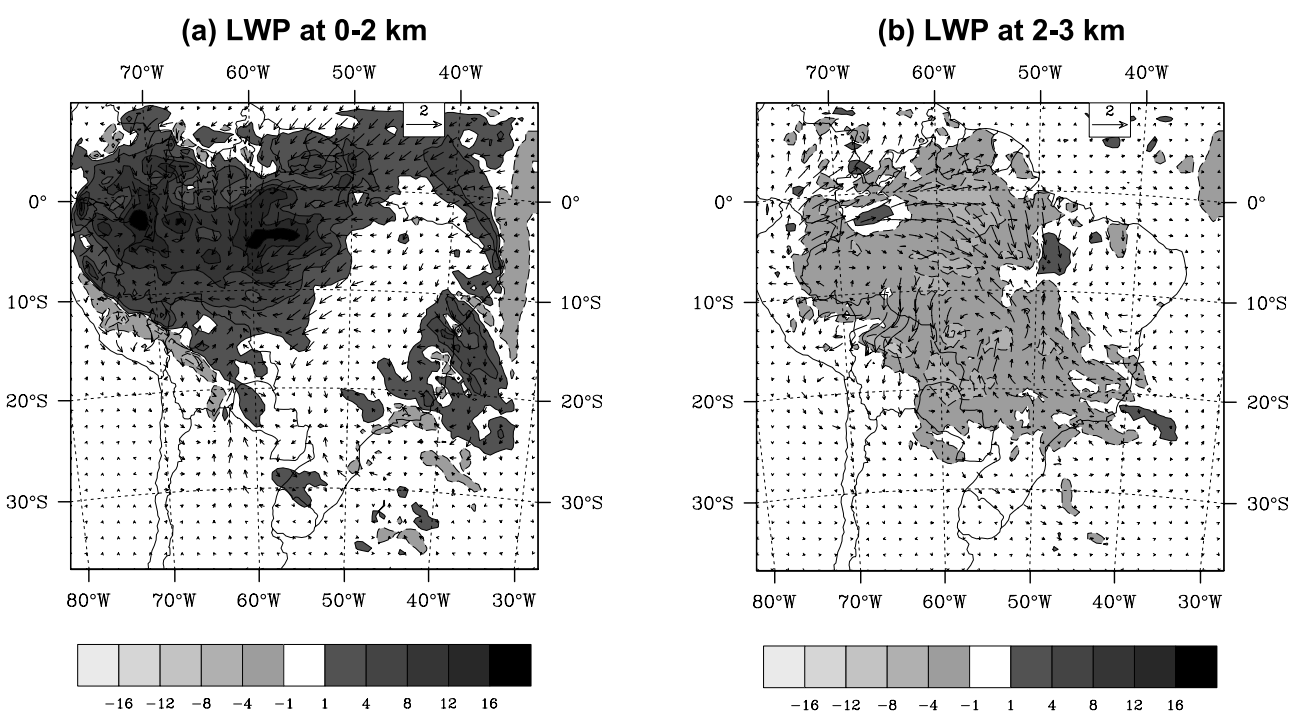

Figure 13. Aerosol induced (a) change in cloud LWP (g m^{-2}) integrated between surface to 2 km and the change of circulation which is indicated by the change of the wind at 1.5 km and (b) changes in cloud LWP between 2 km to 3 km and change of the wind at 3 km.

temperature, hence reducing the lapse rate and enhancing the capping inversion. Weaker turbulence also reduces the height of the daytime PBL. Both processes decrease clouds in the 2 km to 3 km layer right above the top of the PBL.

[32] What could cause the large-scale increase of cloud LWP in the PBL over equatorial Amazonia outside of the smoke area? Figure 13 shows atmospheric circulation perturbations at different levels. This alteration of the regional circulation results from surface cooling in the smoke area that leads to an anomalous lower-level moisture divergence in the smoke area and moisture convergence and higher humidity in the upwind direction of the smoke area in equatorial Amazonia. High humidity in turn increases LWP in the PBL over the equatorial Amazon.

5. Discussion

[33] A sensitivity test assuming an aerosol diurnal variation in RegCM3 was conducted to examine how such a diurnal variation of the aerosol would influence our results. The diurnal variation of AOD is taken from observation of tropical biomass burning smoke as described by *Smirnov et al.* [2002, Figure 2], which shows a 10% lower AOD at 1000 LST (the daytime minimum AOD) and 20% higher AOD at 1600 LST (the daytime maximum AOD) compared to its daily mean. Our test shows that this diurnal change leads to aerosol radiative forcing at the surface 10% smaller in the morning and 10% higher in the afternoon compared to that obtained by using daily mean AOD. The disproportional smaller increase of the aerosol radiative forcing at the surface in the afternoon is due to stronger reduction of clouds compared to that caused by daily mean AOD, which partially compensates the impact of daily maximum AOD on the surface solar flux. The changes in diurnal variation of SH and PBL relative to those forced by daily mean AOD are proportional to that of the surface solar flux. Since observation show that the AOD could exceed 2.0 for single days in September 2002, a sensitivity test with an AOD value of 2.0 in five random days was conducted. It gave a monthly reduction of surface incoming solar radiation of 34 W m^{-2} in the smoke area, and compared to the 30 W m^{-2} simulated using daily mean AOD.

[34] We have also conducted a test using the GOCART aerosol radiative forcing and the initial and boundary conditions for the period of August–October 2001. This simulation showed similar patterns of changes in the surface fluxes induced by smoke aerosols as those obtained from using the initial and boundary conditions for August–October 2002. Evidently, the processes that control the aerosols radiative effect on surface fluxes, clouds, and the transition of monsoon circulation identified in this study are robust and do not change qualitatively with the specific years that might be chosen for simulations.

[35] We have conducted a simulation over a larger domain (100°W ~ 20°W, 35°S ~ 25°N) to test the effect of the lateral boundary conditions on the northwest region. The aerosol induced increase of cloud LWP from 0 to 2 km over the northwest is 18 g m^{-2}, not significantly different from the 20 g m^{-2} obtained from our small domain simulation.

[36] This study suggests somewhat different influences of the direct and semidirect effects of aerosols on the PBL structure and surface fluxes than have been found in previous studies. In particular, atmospheric single column models without inclusion of cloud processes have shown that strongly absorbing aerosols (SSA = 0.8) would raise the daytime PBL height [*Yu et al.*, 2002]. However, the daytime PBL height in this study decreases by about 10%. Decrease of cloudiness in early afternoon also partially compensates for the smoke aerosol effects, leading to a stronger influence of the smoke aerosols on the surface in later morning than in early afternoon. Aerosol absorption stabilizes the PBL. This stabilization could be disturbed by surface heating of the biomass fires, which may cause a net increase of the PBL height. Since fire has not been included in the model, our results may not be applicable in a region of active fire. In addition, the vertical distribution of absorbed aerosol in the convective PBL is important for determination of cloudiness reduction [*Feingold et al.*, 2005] and can modify the PBL height. Thus our results might change if the vertical structure of the aerosol layer were very different from that assumed in our simulations.

[37] By prescribing a uniform smoke aerosol forcing over most of the Amazon region (2°S ~ 22°S, 44°W ~ 70°W, excluding the Andes mountains), *Liu* [2005] has simulated a basin-wide reduction of cloud LWP over smoke area that he attributed to a weaker upward water transport from the PBL to the cloud layer and anomalous subsidence due to smoke. Our simulation uses observed spatial distribution of AOD and provides a more realistic Bowen ratio for the surface fluxes. Our results suggest a reduction of LWP in the smoke area, but an increase of LWP in the equatorial Amazon. The reduction of the LWP in the smoke area is due to a weakened southward moisture transport to this area and a shallower daytime PBL. The former would slow down the building up of lower troposphere moisture, thus convective available energy (CAPE), whereas the latter would reduce the probability for surface air to reach the level of free convection. Both such changes could reduce the probability of atmospheric convection, a primary driver for transition from dry season to monsoon circulation. The reduction of the surface solar and sensible fluxes causes anomalous low-level moisture divergence in the southern Amazon in the smoke area and anomalous moisture convergence in equatorial Amazonia, leading to a dipole of LWP change and a weakening of the transition from dry to wet monsoon circulation.

6. Conclusions

[38] We have applied the regional climate model RegCM3 to examine over Amazonia the smoke aerosol direct and semidirect effect during a dry to wet transition season (August–October). By modifying the soil and plant root parameters and by adding soil water to mitigate the dry bias of soil moisture in the RegCM3, we are able to significantly reduce the discrepancies between the modeled diurnal cycle of the surface sensible and latent fluxes and those observed. The modeled changes occur both from the direct radiative effect of the aerosol and from changes in cloudiness. Changes are seen outside of the region of maximum aerosol as a dynamic response. A decrease of cloudiness in early afternoon partially compensates for the direct effects of smoke aerosols. Consequently, the strongest changes of surface flux and the PBL due to direct and

semidirect effects of the smoke aerosols occur in late morning. The reduction of net solar radiation in the smoke area at the surface (20 $\sim$ 35 W m^{-2}) is mainly compensated by a reduction of surface sensible flux (15 $\sim$ 25 W m^{-2}). Reduction of latent flux is only about 30% (5 $\sim$ 15 W m^{-2}) of the sensible flux reduction. Inside the smoke area, cloudiness decreases with a maximum decrease occurring in the layer right above the daytime PBL (2 km to 3 km above the surface). This decrease is presumably due to strong solar radiation absorption by smoke aerosols in this layer and to the reduction in the daytime PBL height and surface sensible fluxes. Outside of the smoke area in equatorial Amazonia, the cloud liquid water path increases with its maximum increase occurring below 2 km within the daytime PBL. An increase of lower-level moisture convergence in this region appears to be responsible for the increase of both specific and relative humidity in the PBL. Smoke aerosols, probably through their surface cooling, cause an increase of low-level moisture divergence in the smoke center and a compensating moisture convergence in equatorial Amazonia. Such a regional circulation change would delay the normal circulation transition from dry season to monsoon onset.

[39] **Acknowledgments.** This work is supported by the NASA Earth system science research using data and products from Terra, Aqua, and ACRIMSAT NNG04GK90G and NNG04GB89G projects. We thank Susan Ryan for editorial assistance.

References

Ackerman, S., O. B. Toon, D. E. Stevens, A. J. Heymsfield, V. Ramanathan, and E. J. Welton (2000), Reduction of tropical cloudiness by soot, *Science*, *288*, 1042–1047, doi:10.1126/science.288.5468.1042.

Andreae, M. O., D. Rosenfeld, P. Artaxo, A. A. Costa, G. P. Frank, K. M. Longo, and M. A. F. Silva-Diaz (2004), Smoking rain clouds over the Amazon, *Science*, *303*, 1337–1341, doi:10.1126/science.1092779.

Betts, A. K., and C. Jakob (2002), Study of diurnal cycle of convective precipitation over Amazonia using a single column model, *J. Geophys. Res.*, *107*(D23), 4732, doi:10.1029/2002JD002264.

Briegleb, B. (1992), Delta-Eddington approximation for solar radiation in the NCAR community climate model, *J. Geophys. Res.*, *97*(D7), 7603–7612, doi:10.1029/92JD00291.

Chand, D., P. Guyon, P. Artaxo, O. Schmid, G. P. Frank, L. V. Rizzo, O. L. Mayol-Bracero, L. V. Gatti, and M. O. Andreae (2006), Optical and physical properties of aerosols in the boundary layer and free troposphere over the Amazon Basin during the biomass burning season, *Atmos. Chem. Phys.*, *6*, 2911–2925.

Charlson, R. J., S. E. Schwartz, J. H. Hales, R. D. Cess, J. A. Coakley Jr., J. E. Hansen, and D. J. Hofmann (1992), Climate forcing by anthropogenic aerosols, *Science*, *255*, 423–430, doi:10.1126/science.255.5043.423.

Chin, M., P. Ginoux, S. Kinne, O. Torres, B. Holben, B. N. Duncan, R. V. Martin, J. A. Logan, A. Higurashi, and T. Nakajima (2002), Tropospheric aerosol optical thickness from the GOCART model and comparisons with satellite and Sun photometer measurements, *J. Atmos. Sci.*, *59*, 461–483, doi:10.1175/1520-0469(2002)059<0461:TAOTFT>2.0.CO;2.

da Rocha, H. R., M. L. Goulden, S. D. Miller, M. C. Menton, D. V. O. L.Pinto, H. C. de Freitas, and M. E. S. A.Figueira (2004), Seasonality of water and heat fluxes over a tropical forest in eastern Amazonia, *Ecol. Appl.*, *14*(4), S22–S32.

Dickinson, R., A. Henderson-Sellers, and P. J. Kennedy (1993), *Biosphere-atmosphere transfer scheme (BATS) version le as coupled to the NCAR community climate model*, *NCAR Tech. Note TN-387+STR*, Natl. Cent. for Atmos. Res., Boulder, Colo.

Dubovik, O., B. Holben, T. Eck, A. Smirnov, Y. Kaufman, M. King, D. Tanré, and I. Slutsker (2002), Variability of absorption and optical properties of key aerosol types observed in worldwide locations, *J. Atmos. Sci.*, *59*, 590–608, doi:10.1175/1520-0469(2002)059<0590:VOAAOP>2.0.CO;2.

Feingold, G., H. Jiang, and J. Y. Harrington (2005), On smoke suppression of clouds in Amazonia, *Geophys. Res. Lett.*, *32*, L02804, doi:10.1029/2004GL021369.

Fu, R., B. Zhu, and R. E. Dickinson (1999), How do the atmosphere and land surface influence seasonal changes of convection in the tropical Amazon?, *J. Clim.*, *12*, 1306–1321, doi:10.1175/1520-0442(1999)012<1306:HDAALS>2.0.CO;2.

Gash, J. H. C., and C. A. Nobre (1997), Climatic effect of Amazonian deforestation: Some results from ABRACOS, *Bull. Am. Meteorol. Soc.*, *78*, 823–830, doi:10.1175/1520-0477(1997)078<0823:CEOADS>2.0.CO;2.

Goulden, M. L., S. D. Miller, H. R. da Rocha, M. C. Menton, H. C. de Freitas, M. E. S. A.Figueira, and C. A. D. de Sousa (2004), Diel and seasonal patterns of tropical forest CO_2 exchange, *Ecol. Appl.*, *14*(sp4), 42–54, doi:10.1890/02-6008.

Grell, G. A. (1993), Prognostic evaluation of assumptions used by cumulus parameterizations, *Mon. Weather Rev.*, *121*, 764–787, doi:10.1175/1520-0493(1993)121<0764:PEOAUB>2.0.CO;2.

Grell, G. A., J. Dudhia, and D. R. Stauffer (1994), A description of the fifth-generation Penn State/NCAR mesoscale model (MM5), *NCAR Tech. Note TN-398+STR*, 122 pp., Natl. Cent. for Atmos. Res., Boulder, Colo.

Hansen, J., M. Sato, and R. Ruedy (1997), Radiative forcing and climate response, *J. Geophys. Res.*, *102*, 6831–6864, doi:10.1029/96JD03436.

Huang, Y., R. E. Dickinson, and W. L. Chameides (2006), Impact of aerosol indirect effect on surface temperature over east Asia, *Proc. Natl. Acad. Sci. U. S. A.*, *103*, 4371–4376, doi:10.1073/pnas.0504428103.

Johnson, B. T., K. P. Shine, and P. M. Forster (2004), The semi-direct aerosol effect: Impact of absorbing aerosols on marine stratocumulus, *Q. J. R. Meteorol. Soc.*, *130*, 1407–1422, doi:10.1256/qj.03.61.

Kaufman, Y. J., and I. Koren (2006), Smoke and pollution aerosol effect on cloud cover, *Science*, *313*, 655–658, doi:10.1126/science.1126232.

Kaufman, Y. J., A. Setzer, D. Ward, D. Tanre, B. N. Holben, P. Menzel, M. C. Pereira, and R. Rasmussen (1992), Biomass burning airborne and spaceborne experiment in the Amazons (BASE-A), *J. Geophys. Res.*, *97*, 14,581–14,599.

Kaufman, Y. J., et al. (1998), Smoke, Clouds, and Radiation-Brazil (SCAR-B) experiment, *J. Geophys. Res.*, *103*, 31,783–31,808, doi:10.1029/98JD02281.

Kiehl, J. T., J. J. Hack, G. B. Bonan, B. A. Boville, D. L. Williamson, and P. J. Rasch (1998), The National Center for Atmospheric Research Community Climate Model: CCM3, *J. Clim.*, *11*, 1131–1150, doi:10.1175/1520-0442(1998)011<1131:TNCFAR>2.0.CO;2.

Kleidon, A., and M. Heimann (2000), Assessing the role of deep rooted vegetation in the climate system with model simulations: Mechanism, comparison to observations and implications for Amazonian deforestation, *Clim. Dyn.*, *16*, 183–199, doi:10.1007/s003820050012.

Koren, I., Y. J. Kaufman, L. A. Remer, and J. V. Martins (2004), Measurement of the effect of Amazon smoke on inhibition of cloud formation, *Science*, *303*, 1342–1345, doi:10.1126/science.1089424.

Labonne, M., F. M. Bréon, and F. Chevallier (2007), Injection height of biomass burning aerosols as seen from a spaceborne lidar, *Geophys. Res. Lett.*, *34*, L11806, doi:10.1029/2007GL029311.

Landulfo, E., et al. (2003), Synergetic measurements of aerosols over Sao Paulo, Brazil using LIDAR, sunphotometer and satellite data during the dry season, *Atmos. Chem. Phys.*, *3*, 1523–1539.

Liu, Y. Q. (2005), Atmospheric response and feedback to radiative forcing from biomass burning in tropical South America, *Agric. For. Meteorol.*, *133*, 40–53, doi:10.1016/j.agrformet.2005.03.011.

Malhi, Y., E. Pegoraro, A. D. Nobre, M. G. P. Pereira, J. Grace, A. D. Culf, and R. Clement (2002), Energy and water dynamics of a central Amazonian rain forest, *J. Geophys. Res.*, *107*(D20), 8061, doi:10.1029/2001JD000623.

Menon, S., J. Hansen, L. Nazarenko, and Y. Luo (2002), Climate effects of black carbon aerosols in China and India, *Science*, *297*, 2250–2253, doi:10.1126/science.1075159.

Nepstad, D. C., et al. (1994), The role of deep roots in the hydrological and carbon cycles of Amazonian forests and pastures, *Nature*, *372*, 666–669, doi:10.1038/372666a0.

Nobre, P., G. Fisch, da H. R. Rocha, R. F. F. Lyra, da E. P. Rocha, and V. N. Ubarana (1996), Observation of the atmospheric boundary layer in Rondônia, in *Amazonian Deforestation and Climate*, edited by J. H. C. Gash et al., pp. 413–424, John Wiley, Hoboken, N. J.

Pal, J. S., et al. (2007), Regional climate modeling for the developing world—The ICTP RegCM3 and RegCNET, *Bull. Am. Meteorol. Soc.*, *88*, 1395–1409, doi:10.1175/BAMS-88-9-1395.

Procopio, A. S., P. Artaxo, Y. J. Kaufman, L. A. Remer, J. S. Schafer, and B. N. Holben (2004), Multiyear analysis of Amazonian biomass burning smoke radiative forcing of climate, *Geophys. Res. Lett.*, *31*, L03108, doi:10.1029/2003GL018646.

Qian, Y., and F. Giorgi (1999), Interactive coupling of regional climate and sulfate aerosol models over eastern Asia, *J. Geophys. Res.*, *104*, 6477–6499, doi:10.1029/98JD02347.

Rauscher, S. A., A. Seth, B. Liebmann, J. Qian, and S. J. Camargo (2007), Regional climate model - Simulated timing and character of seasonal

rains in South America, *Mon. Weather Rev.*, *135*(7), 2642–2657, doi:10.1175/MWR3424.1.

Reid, J., T. Eck, S. Christopher, R. Koppmann, O. Dubovik, D. Eleuterio, B. Holben, E. Reid, and J. Zhang (2005), A review of biomass burning emissions part III: Intensive optical properties of biomass burning particles, *Atmos. Chem. Phys.*, *5*, 827–849.

Seth, A., and F. Giorgi (1998), The effects of domain choice on summer precipitation simulation and sensitivity in a regional climate model, *J. Clim.*, *11*, 2698–2712, doi:10.1175/1520-0442(1998)011<2698:TEODCO>2.0.CO;2.

Smirnov, A., B. N. Holben, T. F. Eck, I. Slutsker, B. Chatenet, and R. T. Pinker (2002), Diurnal variability of aerosol optical depth observed at AERONET (Aerosol Robotic Network) sites, *Geophys. Res. Lett.*, *29*(23), 2115, doi:10.1029/2002GL016305.

Steiner, A. L., and W. L. Chameides (2005), Aerosol-induced thermal effects increase modelled terrestrial photosynthesis and transpiration, *Tellus, Ser. B*, *57*, 404–411, doi:10.1111/j.1600-0889.2005.00158.x.

Twomey, S. (1977), The influence of pollution on the shortwave albedo of clouds, *J. Atmos. Sci.*, *34*, 1149–1152, doi:10.1175/1520-0469(1977)034<1149:TIOPOT>2.0.CO;2.

von Randow, C., et al. (2004), Comparative measurements and seasonal variations in energy and carbon exchange over forest and pasture in South West Amazonia, *Theor. Appl. Climatol.*, *78*, 5–26, doi:10.1007/s00704-004-0041-z.

Williams, E., and N. Renno (1993), An analysis of the conditional instability of the tropical atmosphere, *Mon. Weather Rev.*, *121*, 21–36, doi:10.1175/1520-0493(1993)121<0021:AAOTCI>2.0.CO;2.

Yu, H., S. C. Liu, and R. E. Dickinson (2002), Radiative effects of aerosols on the evolution of the atmospheric boundary layer, *J. Geophys. Res.*, *107*(D12), 4142, doi:10.1029/2001JD000754.

Yu, H., R. E. Dickinson, M. Chin, Y. J. Kaufman, B. N. Holben, I. V. Geogdzhayev, and M. I. Mishchenko (2003), Annual cycle of global distributions of aerosol optical depth from integration of MODIS retrievals and GOCART model simulations, *J. Geophys. Res.*, *108*(D3), 4128, doi:10.1029/2002JD002717.

Yu, H., et al. (2006), A review of measurement-based assessment of aerosol direct radiative effect and forcing, *Atmos. Chem. Phys.*, *6*, 613–666.

Yu, H., R. Fu, R. E. Dickinson, Y. Zhang, M. Chen, and H. Wang (2007), Interannual variability of smoke and warm cloud relationships in the Amazon as inferred from MODIS retrievals, *Remote Sens. Environ.*, *111*, 435–449, doi:10.1016/j.rse.2007.04.003.

Zhou, M., H. Yu, R. E. Dickinson, O. Dubovik, and B. N. Holben (2005), A normalized description of the direct effect of key aerosols types on solar radiation as estimated from AERONET aerosols and MODIS albedos, *J. Geophys. Res.*, *110*, D19202, doi:10.1029/2005JD005909.

M. Chin, Laboratory for Atmospheres, NASA Goddard Space Flight Center, Greenbelt, MD 20771, USA.

R. E. Dickinson, R. Fu, and Y. Zhang, School of Earth and Atmospheric Sciences, Georgia Institute of Technology, 311 Ferst Drive, Atlanta, GA 30332-0340, USA. (yan.zhang@gatech.edu)

R. N. Juarez, Department of Ecology and Evolutionary Biology, Tulane University, New Orleans, LA 70118, USA.

H. Wang, Wyle Information Systems, Climate Prediction Center, NOAA, Camp Springs, MD 20746, USA.

H. Yu, Goddard Earth Science and Technology Center, University of Maryland, Baltimore County, Baltimore, MD 21228, USA.